EPR of a Jahn-Teller distorted ⟨111⟩ carbon interstitialcy in irradiated silicon*

K. L. Brower
Sandia Laboratories, Albuquerque, New Mexico 87115
(Received 17 October 1973)

An electron-paramagnetic-resonance (EPR) study of irradiated, p-type silicon doped with carbon enriched with ^{13}C has revealed that the Si-G11 spectrum possesses a ^{13}C hyperfine structure. Owing to the complexity and lack of resolution in the observed spectrum, we found it necessary to use a resolution-enhancement technique in order to unravel the angular dependence in the ^{13}C hyperfine spectra. An analysis of the Zeeman and ^{13}C hyperfine interactions indicates that the Si-G11 center consists of a vacancy occupied by two carbon atoms in a positive-charge state. The effects of stress applied at low temperature indicate that the Si-G11 center is distorted by the Jahn-Teller effect from $\mathfrak{C}_{3v}$ symmetry, a configuration in which both carbon atoms are situated near a vacancy and lie on the ⟨111⟩ axis, to $\mathfrak{C}_s$ symmetry, a configuration corresponding to a distorted ⟨111⟩ carbon interstitialcy. The activation energy for electronic reorientation from one Jahn-Teller distortion to another was found to be 0.20 eV. The effects of stress applied at high temperature indicate an atomic reorientation process which occurs with an activation energy of 1.21 eV.

I. INTRODUCTION

Electron-paramagnetic-resonance (EPR) studies have revealed much about the structure and kinetics of defects in electron-,[1,2] neutron-,[3-5] and ion-bombarded[6] silicon. Most of these studies have dealt with the vacancy-associated component of the lattice damage. By comparison, the interstitial-associated component of the lattice damage in silicon is not nearly as well understood. In fact, there is no direct experimental information on the self-interstitial in any material having the diamond lattice. In the case of silicon, experimental evidence suggests that the silicon interstitial (Si_i) is in effect mobile even at 4 K and therefore does not remain in the lattice during a radiation-damage experiment.[1]

To help elucidate this situation, various theoretical calculations have been performed. Singhal[7,8] found that for the Si_i in the tetrahedral or bond-centered interstitial sites there are no defect levels within the band gap, which could be another reason why the Si_i plays such a passive role in lattice-damage effects. Watkins, Messmer, Weigel, Peak, and Corbett[9,10] have performed molecular-orbital cluster calculations using the extended Hückel theory for various configurations of the carbon interstitial in diamond. They concluded that the carbon interstitial in diamond prefers an interstitialcy configuration as against the hexagonal or tetrahedral interstitial sites.

In contrast to the situation regarding self-interstitials, there are some experimental measurements on impurity interstitials in silicon. In particular, EPR studies indicate that the Al_i^+ occupies the tetrahedral interstitial site.[11] In order to account for the production of Al_i^+ at 4 K in silicon, Watkins proposed that the Si_i, which is produced along with the vacancy in the primary radiation-damage event, in effect migrates through the lattice until trapped by a substitutional aluminum ion (Al_s^-). In the trapped state, the Si_i replaces the Al_s^- ejecting it into the interstitial site.[1] In this site, the Al_i^+ is stable to ≈500 K.[2] At ≈500 K, the Al_i^+ is observed to pair with an Al_s^-; the Al_i^+-Al_s^- pair is stable to ≈600 K.[2] This pairing behavior is also exhibited by Ga.[1]

Some years ago, Watkins observed a Zeeman spectrum which he labeled Si-G11.[1] The identity of this center has not previously been established, and no hyperfine spectra belonging to the Zeeman spectrum were reported. Recently, while looking at the lattice damage in p-type silicon doped with carbon enriched with ^{13}C, we discovered that the Si-G11 spectrum possesses two inequivalent ^{13}C hyperfine spectra. We also observed that the Si-G11 center undergoes electronic reorientation from one Jahn-Teller distortion to another. Our analysis of the ^{13}C hyperfine spectra and the reorientation of the Si-G11 center, which is presented in this paper, indicates that the Si-G11 center is a Jahn-Teller distorted ⟨111⟩ carbon interstitialcy. This is the first time that the molecular and electronic structure of a group-IV interstitial complex has been identified in silicon. These results are also important because they tend to corroborate the theoretical predictions of Watkins *et al.*[9,10] regarding the structure of the self-interstitial in the diamond lattice.

II. EXPERIMENT

A. Samples

Two different silicon crystals were used in this EPR study. One crystal of Lopex silicon was doped with ≈3×10^{15} B/cm^2 and contained ≈10^{17} (ordinary

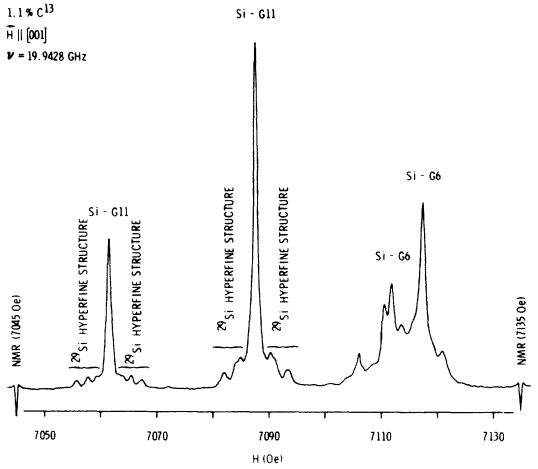

FIG. 1. EPR spectrum at 14 K which was observed in our sample of Lopex silicon containing ordinary carbon and irradiated with 10^{15} n/cm^2.

carbon)/cm^3. Ordinary carbon consists of 98.89% ^{12}C and 1.11% ^{13}C. Although the nuclear spin of ^{12}C is zero, ^{13}C has a nuclear spin of $\frac{1}{2}$. Another crystal of vacuum-float-zone-refined silicon was doped with $\approx 10^{15}$ B/cm^3 and $\approx 10^{7}$ C/cm^3. The carbon used to dope this sample consisted of 60.1% ^{13}C and 39.9% ^{12}C. The Si-$G11$ center could be produced in both of these samples by neutron or electron irradiation at room temperature.[12]

B. Spectra

The EPR spectra observed from the two different crystals are shown in Figs. 1 and 2. Although the Zeeman lines belonging to the Si-$G11$ center are present in both samples, the satellite structure associated with these Zeeman lines is vastly different. In Fig. 1, the satellite structure is dominated by ^{29}Si hyperfine lines because in this sample ^{29}Si is 4.71% naturally abundant whereas ^{13}C is only 1.11% naturally abundant. The intensities of the ^{29}Si hyperfine lines suggest that these interactions arise from pairs of silicon sites which appear to be equivalent. In Fig. 2, the satellite structure is dominated by ^{13}C hyperfine lines (denoted by α, β, and $\alpha\beta$) because the carbon in this sample is enriched with ^{13}C to 60.1%. The ^{13}C hyperfine spectrum indicates that there are two inequivalent carbon sites in the Si-$G11$ center.

The angular dependence in the Si-$G11$ Zeeman spectrum indicates that this defect has $\mathfrak{C}_s$ symmetry, which implies that the two carbon atoms lie in a $\{110\}$ plane having reflection symmetry. Consequently, the 18 lines composing the Si-$G11$ spectrum in Fig. 2 split into 63 lines when $\vec{H}$ is rotated off from any high-symmetry direction in the (110) plane. These 63 lines are contained within an interval of $\lesssim 80$ Oe. The complexity of this spectrum is further compounded by overlap with the Si-$G6$ (positive-divacancy) spectrum. Our initial attempts at unravelling the angular dependence in the ^{13}C hyperfine lines failed because the lines were not sufficiently resolved. We were also unable to observe any ^{13}C electron-nuclear double resonances.

These difficulties prompted us to utilize a technique called resolution enhancement. In the method we used,[13] the resolution of an EPR spectrum can be enhanced by adding to the original spectrum, f, admixtures of its even derivatives. In order to carry out this procedure, we recorded our EPR spectra on magnetic tape at a rate of ≈ 100 (data points)/Oe. Using a CDC 6600 computer, smoothing and differentiation was accomplished by least-squares-fitting 49 data points, which corresponded to a segment in a spectrum, to a parabola and calculating the derivative of the parabola at the midpoint. By taking successive segments, the derivative of the original spectrum and subsequently the $(n+1)$th derivative of the nth derivative were generated. The resolution-enhanced spectrum, F, was then specified by the formula

$$F = f - 0.1\, d^2f/dH^2 + 0.004\, d^4f/dH^4 . \qquad (1)$$

The coefficients specifying the admixture of the even derivatives, which give optimum visual resolution in F, are peculiar to the linewidth of the individual resonances and, in our case, were determined by trial and error. An example showing the results of this analysis is illustrated in Fig. 3. With this method we were able to decrease our linewidth by a factor of 2 to 3. Subsequently, we were able to unravel the angular dependence in the Si-$G11$ ^{13}C hyperfine spectra.

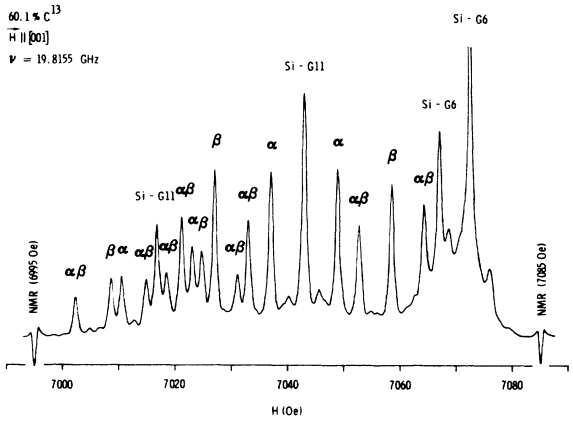

FIG. 2. EPR spectrum at 15 K which was observed in our vacuum-float-zone-refined silicon doped with carbon enriched with ^{13}C to 60.1% and irradiated with 5×10^{16} 2-MeV e^-/cm^2.

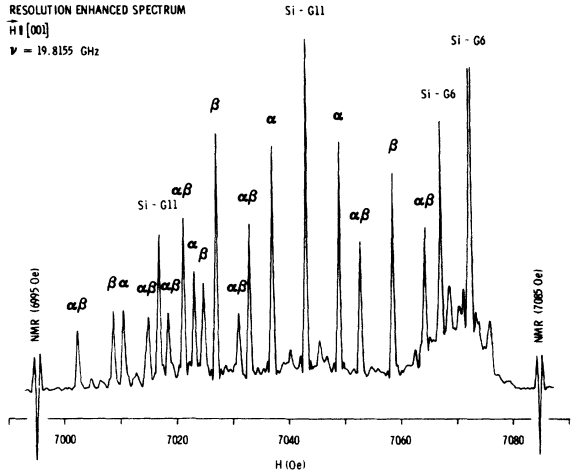

FIG. 3. Resolution enhancement of the spectrum in Figure 2.

C. Stress effects

Whether or not a defect is distorted from a higher symmetry by the Jahn-Teller effect can usually be determined by studying the effects of stress on the center at low temperature. Depending upon the orientation of a defect in a strain field, the Jahn-Teller distortion of a defect can be enhanced, thereby lowering its energy still further, or the Jahn-Teller distortion can be partially compensated, thereby raising the energy of the defect. Defects of a particular kind which have undergone Jahn-Teller distortion can be divided into subsets each consisting of defects which differ in orientation by only a simple electronic reorientation. On the other hand, the transposition of a defect from one

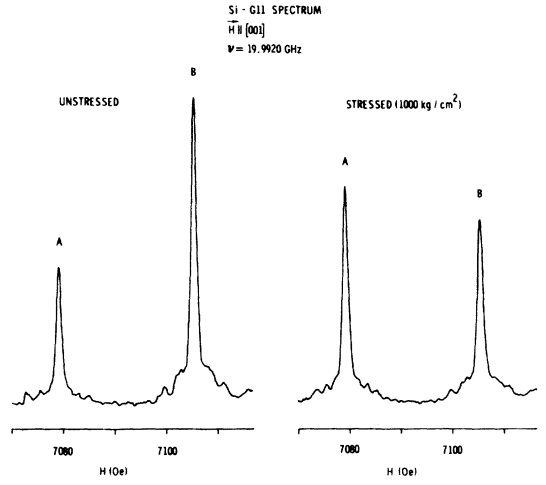

FIG. 4. Effects of low-temperature stress. The Si-*G*11 spectrum was recorded at 15 K without the effects of stress and with uniaxial stress applied *in situ* along the [$\bar{1}$10] direction beforehand at 80 K and released at 15 K. This sample of Lopex silicon was irradiated with 3 $\times 10^{13}$ n/cm^2.

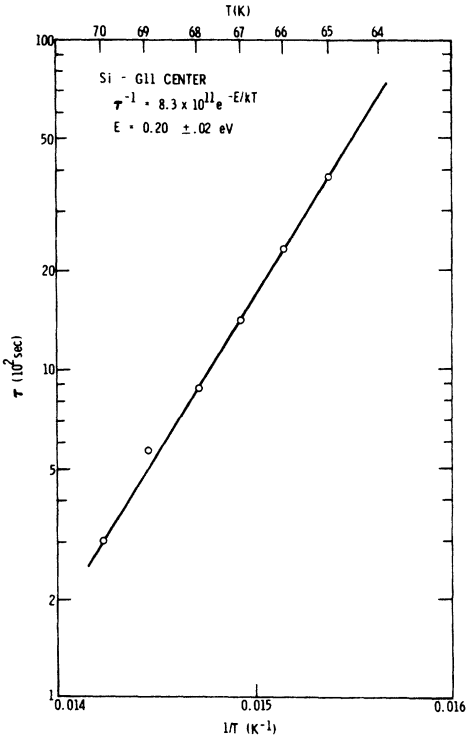

FIG. 5. Plot of lifetime for electronic reorientation vs reciprocal temperature for the Si-*G*11 center.

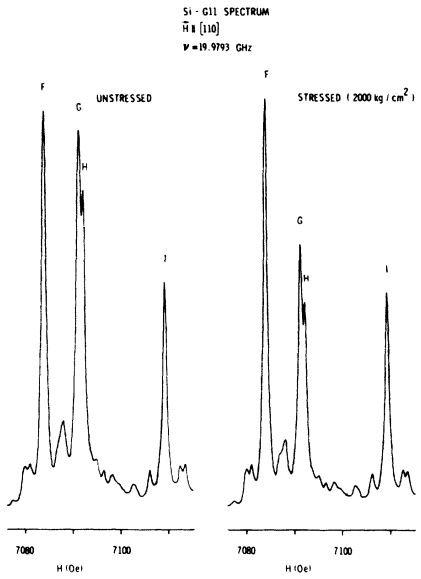

FIG. 6. Effects of high-temperature stress. The Si-*G*11 spectrum was recorded at 15 K without stress and with uniaxial stress applied along the [$\bar{1}$10] direction at 175 °C and removed at room temperature. This sample of Lopex silicon was irradiated with 10^{15} n/cm^2.

subset to another requires an atomic rearrangement. The activation energy for electronic processes is small compared to that for atomic processes. Consequently, electronic processes, which are usually indicative of Jahn-Teller effects, achieve thermal equilibrium at relatively low temperatures, and atomic processes, which involve a rearrangement of the atoms in the defect, achieve thermal equilibrium at relatively high temperatures.

1. Low-temperature stress effects

The contrast in Si-*G*11 spectra without stress and with stress applied *in situ* at low temperature is shown in Fig. 4. The difference in the ratio of the intensities of resonances *A* and *B* before stress (*A* : *B* : : 1 : 2) and after stress (*A* : *B* : : 1 : 1) indicates that there has been a preferential alignment of the Si-*G*11 centers with respect to the strain field. Since there is also another reorientation process that occurs at higher temperatures, this low-temperature reorientation is due only to electronic rearrangements and is indicative of a Jahn-Teller distortion in the Si-*G*11 center. It is also important to note that each subset of defect orientations which differ by only a simple electronic reorientation contains defect orientations which give rise to both resonances *A* and *B*. The fact that the Si-*G*11 center can reorient from *A* to *B* without an atomic rearrangement tells us something about the symmetry of the Si-*G*11 center before it is lowered by the Jahn-Teller effect (see Sec. IV).

It is also possible to measure the rate at which a stress-induced polarization of defect orientations recovers as a function of time and temperature. These data are summarized in Fig. 5 and indicate that the activation energy for this electronic process is 0.20 ± 0.02 eV. Because a polarization in defect orientations can be achieved with ≈30 times more holes than Si-*G*11 centers (all the Si-*G*11 centers are supplied with a hole and are paramagnetic), this activation energy is interpreted as the activation energy for electronic reorientation (as against the activation energy for hole redistribution, in which case the activation energy would correspond to the position of the defect level above the valence band).

2. High-temperature stress effects

The contrast in the Si-*G*11 spectra without and with stress applied at high temperature is shown in Fig. 6. In this case, the sample was heated to 175 °C and then subjected to uniaxial stress of 2000 kg/cm^2 along the [1$\bar{1}$0] direction. This stress was not removed until the sample had cooled to room temperature. At room temperature, all the electronic processes promptly relax to thermal equilibrium, and only the effects of atomic rearrangements induced by the stress remain frozen in. In particular, the fact that the relative intensity of *F* with respect to *I* remains unchanged in Fig. 6 suggests that these resonances (*F*, *I*) are associated with defect orientations which differ by only an electronic reorientation. The same is also true of resonances *G* and *H*. On the other hand, the change in the relative intensity of resonances *F* + *I* with respect to *G* + *H* in Fig. 6 is indicative of a preferential alignment in Si-*G*11 centers achieved through atomic rearrangements. These results tell us something about the structure of the Si-*G*11 center (see Sec. IV).

Again, the rate at which the stress-induced polarization of defects recovered was measured by EPR as a function of time and temperature. The samples were annealed in a temperature-controlled, stirred oil bath. The temperature of the oil bath was stable to ±0.1 °C with respect to time and position in the bath and was measured by means of a mercury thermometer. The results of these measurements are summarized in Fig. 7. A least-squares fit of the Arrhenius equation to these data indicates that the activation energy for an atomic reorientation of the Si-*G*11 center is 1.21 ± 0.08 eV.

D. Annealing

The 20-min isochronal annealing of the Si-*G*11 center is shown in Fig. 8. At ≈200 °C a new cen-

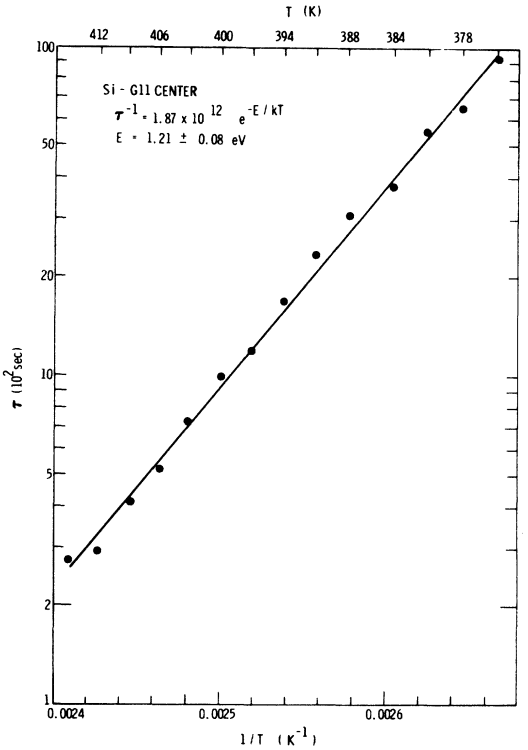

FIG. 7. Plot of lifetime for atomic reorientation vs reciprocal temperature for the Si-*G*11 center.

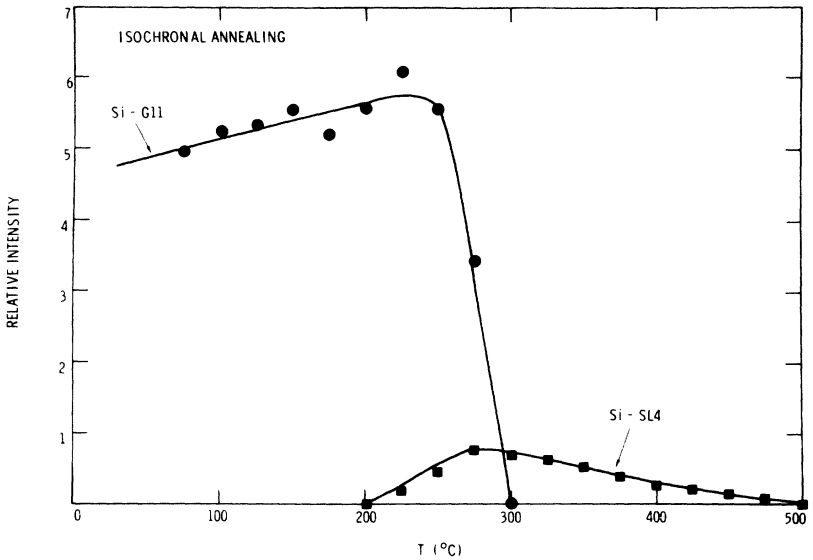

FIG. 8. Relative intensities of the Si-*G*11 and Si-*SL*4 centers vs temperature at which 20-min isochronal anneals were performed from 75 to 500°C.

ter, labeled Si-*SL*4, appears.[14] Although the Si-*SL*4 spectrum was observed in our silicon sample enriched with ^{13}C, no resolved ^{13}C hyperfine lines were observed in this spectrum.

III. ANALYSIS

A. Spin Hamiltonian

The spin Hamiltonian which is appropriate for describing the EPR spectra associated with the various isotopic carbon configurations of the Si-*G*11 center is

$$\mathcal{H} = \mu_B \vec{H} \cdot \overleftrightarrow{g} \cdot \vec{S} + \sum_k \vec{S} \cdot \overleftrightarrow{A}_k \cdot \vec{I}_k \,. \tag{2}$$

The Zeeman interaction and the kth hyperfine interaction are characterized by the $\overleftrightarrow{g}$ and $\overleftrightarrow{A}_k$ coupling tensors, respectively; μ_B is the Bohr magneton. Since this defect is a $S = \frac{1}{2}$ center and the hyperfine interactions are small, the nuclear Zeeman interaction has negligible effect on the observed hyperfine spectra and is therefore omitted from Eq. (2).

The eigenvalues to Eq. (2) were determined by perturbation theory to second order. In this perturbation analysis, the electron-spin operator $\vec{S}$ was quantized along $\vec{H} \cdot \overleftrightarrow{g}$, and the nuclear-spin operator $\vec{I}_k$ was quantized in such a direction that the coefficients to the spin terms $S_z I_{+k}$ and $S_z I_{-k}$ were zero. (S_z is parallel to $\vec{H} \cdot \overleftrightarrow{g}$.)

The $\overleftrightarrow{g}$ tensor was determined by fitting the calculated Zeeman spectrum to the observed Zeeman spectrum by a least-squares method. The results of this analysis on the $\overleftrightarrow{g}$ tensor are tabulated in Table I and agree within experimental error to

TABLE I. Tabulation of the $\overleftrightarrow{g}$ and $\overleftrightarrow{A}_k$ tensors as determined by a numerical analysis of the Si-*G*11 spectrum measured at ≈20 GHz and 15 K. The principal axes for these coupling tensors are defined in Fig. 9.

$\overleftrightarrow{g}$ tensor (Ref. 1) ± 0.0002

g_{rr}	g_{ss}	g_{tt}	ω
2.0179_5	2.0076_3	2.0126_9	-8.1_0

$\overleftrightarrow{A}$ tensor (10^{-4} cm^{-1}) ± 0.2

k	$A_{u_k u_k}$	$A_{v_k v_k}$	$A_{w_k w_k}$	ψ_k
$^{13}C_\alpha$	12.8_7	10.4_9	10.5_5	-43.1_8
$^{13}C_\beta$	43.4_6	7.8_6	5.7_4	72.3_1

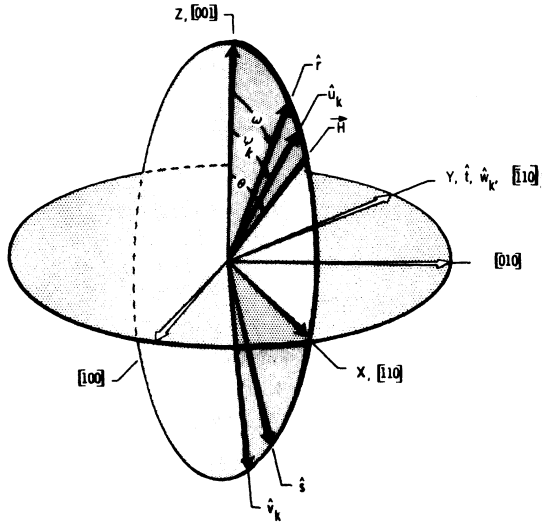

FIG. 9. Definition of the coordinate axes for the $\overleftrightarrow{g}$ and $\overleftrightarrow{A}_k$ tensors in relation to various crystallographic directions.

those determined previously by Watkins.[1] The anisotropy in the $\overleftrightarrow{g}$ tensor is consistent with the Si-*G*11 center having $\mathfrak{C}_s$ symmetry.

The $^{13}C_\alpha$ and $^{13}C_\beta$ hyperfine tensors were determined by fitting the observed spectra to the calculated spectra by a least-squares method. Only those resonances which could be identified unambiguously for the magnetic field $\vec{H}$ along high-symmetry directions and which were unperturbed in magnetic field position by other resonances were included in the least-squares fit. The numerical values for the $^{13}C_\alpha$ and $^{13}C_\beta$ hyperfine tensors are tabulated in Table I. The relationship between the crystalline directions and the directions of the principal axes of the coupling tensors is illustrated in Fig. 9. The angular dependences in the observed and calculated spectra for the four isotopic carbon configurations of the Si-*G*11 center are shown in Fig. 10. The original data consisted of the superposition of the data in Fig. 10 plus the data arising from the Si-*G*6 spectrum.

B. ^{13}C hyperfine interactions

From the ^{13}C hyperfine tensors tabulated in Table I, one can now proceed to deduce the *s* and *p* character of the wave function for the paramagnetic electron in the vicinity of the two carbon atoms. The Hamiltonian for the hyperfine interaction[15] is

$$\mathcal{H}_{hf}=\sum_k \left\{ \frac{16}{3}\pi\mu_B \frac{\mu_k}{I_k}\delta(\vec{R}_k-\vec{r})\vec{S}\cdot\vec{I}_k - 2\mu_B\frac{\mu_k}{I_k}\left[\frac{\vec{S}\cdot\vec{I}_k}{r^3}-\frac{3(\vec{S}\cdot\vec{r}_k)(\vec{I}_k\cdot\vec{r}_k)}{r^5}\right] + 2\mu_B\frac{\mu_k}{I_k}\frac{\vec{L}\cdot\vec{I}_k}{r^3}\right\}, \quad (3)$$

where μ_B is the Bohr magneton, μ_k is the magnetic moment for the *k*th nucleus, $\vec{r}$ is the position vector for the paramagnetic electron, and $\vec{R}_k$ is the position vector for the *k*th nucleus. Since the orbital angular momentum $\vec{L}$ in the Si-*G*11 center is essentially quenched, the contribution to the hyperfine interaction arising from the orbital term in Eq. (3) is negligible. It has been demonstrated that a partial, semiquantitative description of the wave function for the paramagnetic electron in a defect can be deduced from the hyperfine interactions. As is usually done,[1] the wave functions associated with the defect are represented by linear combinations of atomic orbitals consistent with symmetry. In the case of the Si-*G*11 center, which has $\mathfrak{C}_s$ symmetry, a molecular orbital which transforms as Γ_1 can be written as

$$\Psi(\Gamma_1)=\eta_\alpha(a_{\alpha1}\psi_{2s}+a_{\alpha2}\psi_{2p_X}+a_{\alpha3}\psi_{2p_Z}) + \eta_\beta(a_{\beta1}\psi_{2s}+a_{\beta2}\psi_{2p_X}+a_{\beta3}\psi_{2p_Z})+\cdots . \quad (4)$$

The constant η_k specifies the fraction of the normalized *s*, *p* hybrid orbital localized on site *k*. By calculating matrix elements of $\langle\Psi(\Gamma_1)|\mathcal{H}_{hf}|\Psi(\Gamma_1)\rangle$,

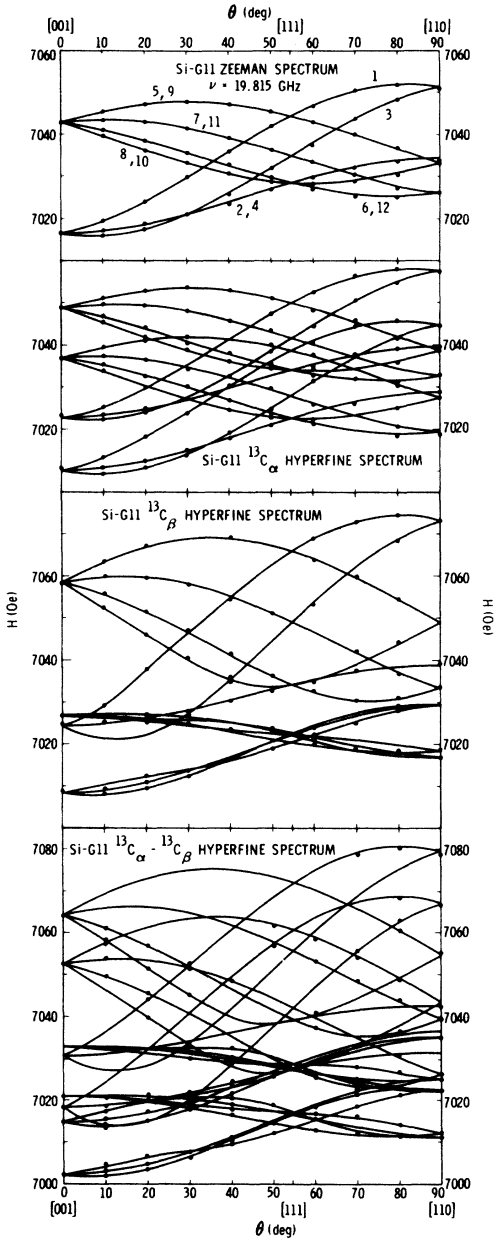

FIG. 10. Plots of the Si-*G*11 Zeeman and ^{13}C hyperfine spectra. The solid lines correspond to the hypothetical spectra for the various isotopic configurations of the defect which are specified by the spin Hamiltonian in Eq. (1) and the coupling tensors in Table I. The dots are representative of the recorded data, which was taken every 2°. The number associated with the various lines in the Zeeman spectrum specify particular coordinate frames which are defined in Table IV. Although four distinct plots are presented here for purposes of clarity, the raw experimental data consisted of the superposition of the data in these four plots (for example, see Figs. 2 and 3).

TABLE II. Tabulation of various atomic parameters for C° and C⁺. The theoretical values were calculated by Cowan (Ref. 16) using a Hartree–Fock computer code (Ref. 18). The experimental value for C° was determined by atomic-beam magnetic resonance (Ref. 17).

	$\lvert\psi_{2s}(0)\rvert^2$ (10^{24} cm^{-3})		$\langle r^{-3}\rangle_{2p}$ (10^{24} cm^{-3})	
	C°	C⁺	C°	C⁺
Theoretical	18.77	21.56	11.21	14.99
Experimental	•••	•••	11.58	15.48 (extrapolated)

it is possible to relate the hyperfine coupling tensors in Eq. (2) to the various parameters in Eq. (4). To a first approximation in which the overlap of atomic orbitals from neighboring atoms is neglected, the relationships are

$$A_{XXk} = F\eta_k^2 a_{k1}^2 + G\eta_k^2(-2a_{k2}^2 + a_{k3}^2), \tag{5}$$

$$A_{YYk} = F\eta_k^2 a_{k1}^2 + G\eta_k^2(a_{k2}^2 + a_{k3}^2), \tag{6}$$

$$A_{ZZk} = F\eta_k^2 a_{k1}^2 + G\eta_k^2(a_{k2}^2 - 2a_{k3}^2), \tag{7}$$

$$A_{XZk} = -\tfrac{15}{4} G\eta_k^2 a_{k2} a_{k3}, \tag{8}$$

$$F = \tfrac{16}{3}\pi\mu_B(\mu_k/I_k)\lvert\psi_{2s}(0)\rvert^2, \tag{9}$$

and

$$G = -\tfrac{4}{5}\mu_B(\mu_k/I_k)\langle r^{-3}\rangle_{2p}. \tag{10}$$

The subscripts X, Y, Z are defined in Fig. 9. In order to solve this set of equations, $\lvert\psi_{2s}(0)\rvert^2$ and $\langle r^{-3}\rangle_{2p}$ for carbon need to be specified. Various theoretical and experimental values for these atomic parameters are listed in Table II. Because the Si-$G11$ center is positively charged, the charge on each of the carbon atoms ranges from 0 to +1. Using the theoretical values[16] for $\lvert\psi_{2s}(0)\rvert^2$ and the experimental values[17] for $\langle r^{-3}\rangle_{2p}$, the various parameters in the molecular orbital Ψ were evaluated. These results, which reveal the s and p character of the paramagnetic electron as well as its localization on the two carbon atoms in the Si-$G11$ center, are tabulated in Table III.

TABLE III. Tabulation of the numerical values for the various parameters in the molecular orbital of Eq. (4) as calculated from Eqs. (5)–(10) and the data in Table II. Note that $N_k^2 = a_{k2}^2 + a_{k3}^2$ and that $\gamma_k = \tan^{-1}(a_{k2}/a_{k3})$; γ_k is the angle between the [001] direction and the axis of the p orbital in the (110) plane containing the two carbon atoms.

	η_k^2	a_{k1}^2	a_{k2}^2	a_{k3}^2	N_k^2	γ_k
C_α^0	0.018	0.062	0.44	0.50	0.94	−43.08
C_α^+	0.014	0.081	0.42	0.49	0.92	−43.08
C_β^0	0.31	0.0062	0.86	0.13	0.99	68.38
C_β^+	0.23	0.0083	0.86	0.13	0.99	68.38

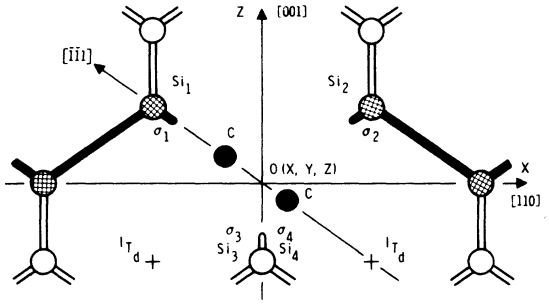

FIG. 11. ⟨111⟩ carbon interstitialcy in irradiated silicon without Jahn-Teller distortion. The solid circles represent the two carbon atoms located on the [1̄11] axis, and the shaded circles represent neighboring silicon atoms in the [110] plane. The open circles correspond to pairs of neighboring silicon atoms located above and below the [110] plane. In particular, Si_3 is above and Si_4 is below the XZ plane. I_{Td} corresponds to the tetrahedral intersititial site.

IV. STRUCTURE OF THE Si-$G11$ CENTER

Our model for the Si-$G11$ center without Jahn-Teller distortion is illustrated in Fig. 11. With Jahn-Teller effects, the carbon pair is believed to correspond to one of the configurations in Fig. 12. The various aspects of our EPR measurements which corroborate this model of the Si-$G11$ center are discussed in this section.

The fact that the Si-$G11$ center has a spin of $\frac{1}{2}$ and incorporates atoms with even Z, as evidenced by the hyperfine structure, indicates that it is in an odd-charge state. Since the defect is found in p-type silicon and goes from the paramagnetic,

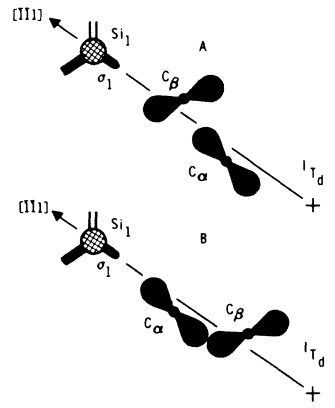

FIG. 12. Illustration of the two possibilities (A, B) for the electronic structure of the Jahn-Teller distorted ⟨111⟩ carbon interstitialcy. Of course, only one of these configurations corresponds to the actual defect. I_{Td} corresponds to the tetrahedral interstitial site.

odd-charge state to the diamagnetic, even-charge state at higher radiation fluences, the Si-*G*11 center is singly, positively charged.

The anisotropies in the $\overleftrightarrow{g}$ tensor and ^{13}C hyperfine tensors indicate that the Si-*G*11 center has $\mathfrak{C}_s$ symmetry; in particular, the (110) plane containing the two carbon atoms is a reflection plane of symmetry. From Table I, one sees that the directions of the principal axes of g_{rr} and g_{ss} are almost parallel with the Z and X axes in Fig. 9 and 11. Since the $\overleftrightarrow{g}$ tensor reflects information about the overall symmetry of the defect wave function and its environment, the $\overleftrightarrow{g}$ tensor appears to be indicative of a defect having nearly $\mathfrak{C}_{2v}$ symmetry. Furthermore, the anisotropy of the $\overleftrightarrow{g}$ tensor relative to the free-electron g value of 2.0023 is

$$\Delta\overleftrightarrow{g} = 0.0053 \begin{pmatrix} \hat{r} \\ \hat{s} \\ \hat{t} \end{pmatrix}^{\dagger} \begin{pmatrix} 2.962 & 0 & 0 \\ 0 & 1.000 & 0 \\ 0 & 0 & 1.962 \end{pmatrix} \begin{pmatrix} \hat{r} \\ \hat{s} \\ \hat{t} \end{pmatrix}. \tag{11}$$

Except for a rotation of 90° about the $\hat{X} \parallel [110]$ direction, the anisotropy in the $\overleftrightarrow{g}$ tensor of the Si-*G*11 center is very similar to that of the Si-*SL*1 center,[3] which consists of an oxygen atom displaced along the [001] direction from a vacant lattice site. The choice we are faced with is whether the carbon pair is located interstitially or in combination with a vacancy. Since the Jahn-Teller effect distorts the Si-*G*11 center from $\mathfrak{C}_{3v}$ symmetry, as discussed below, we would expect the $\overleftrightarrow{g}$ tensor for the Si-*G*11 center to be more nearly axially symmetric, particularly if the carbon atoms were both located interstitially near the ⟨111⟩ axis. In our opinion, the symmetry and anisotropy in the observed $\overleftrightarrow{g}$ tensor suggests that the Si-*G*11 center consists of a vacancy occupied by a carbon pair as illustrated in Figs. 11 and 12. Since there are two carbon atoms which share a vacancy in Fig. 11, we refer to this defect as a carbon interstitialcy.

The Jahn-Teller effect reveals additional features concerning the position of the carbon atoms in the Si-*G*11 center. Our experimental measurements indicate that under the influence of stress applied at low temperature the relative intensities of the resonances in the Si-*G*11 spectrum are altered when $\vec{H}$ is parallel to a ⟨001⟩ direction. With respect to Fig. 11, this means that the defect undergoes electronic reorientations by rotations of ±120° about the $[\bar{1}\,\bar{1}1]$ direction. Furthermore, the Si-*G*11 center does not undergo electronic reorientation by rotations of 180° about the [001] axis. Since an atomic rearrangement is not involved, the two carbon atoms must lie near the axis of rotation. This means that without the Jahn-Teller effect, the Si-*G*11 center has $\mathfrak{C}_{3v}$ symmetry about a ⟨111⟩ axis and not $\mathfrak{D}_{2d}$ symmetry about a ⟨001⟩ axis. The implication regarding this distinction in the undistorted symmetry is that the Si-*G*11 center is basically a carbon pair located on a ⟨111⟩ axis, as illustrated in Fig. 11, and not a ⟨001⟩ axis.

In this respect, it is interesting to note that several carbon centers studied by Newman and Bean[19] with infrared absorption spectroscopy in silicon irradiated at low temperature also have axial symmetry. They concluded that many of these centers involve a carbon interstitial. However, the centers they studied all anneal at $\lesssim 300$ K so that their relationship to the Si-*G*11 center is rather obscure.

So far we have established that the two carbon atoms lie in a {110} plane and are distorted off from a ⟨111⟩ axis by the Jahn-Teller effect. From Fig. 11 it is obvious that there are two ⟨111⟩ axes in each of the {110} planes. With respect to Fig. 11 a question arises as to whether the two carbon atoms lie near the $[\bar{1}\,\bar{1}1]$ as shown or the [111] axis. There is a difference. If the two carbon atoms are distorted off from the $[\bar{1}\,\bar{1}1]$ axis, then the p orbital of C_α (C_β) is nearly parallel (perpendicular) to the $[\bar{1}\,\bar{1}1]$ carbon axis as shown in Fig. 12. On the other hand, if the two carbon atoms are distorted off from the [111] axis, then the p orbital of C_α (C_β) is nearly perpendicular (parallel) to the [111] carbon axis. These two alternatives exist because the orientations of the p orbitals as deduced from the ^{13}C hyperfine interactions are specified with respect to XYZ in Fig. 11, which is defined as coordinate frame 1.

The axis along which the carbon atoms actually lie can be identified from the effects on the Zeeman spectrum due to stress applied at high temperature.[20,21] With respect to the data in Fig. 6, the application of stress at 175 °C along the $[\bar{1}10]$ direction corresponds to applying that stress along the Y direction in Fig. 11. It is evident from symmetry considerations that with a $[\bar{1}10]$ uniaxial stress the energy of a carbon pair on either the $[\bar{1}\,\bar{1}1]$ or [111] axis will be different from that for a carbon pair on either the $[1\bar{1}\,\bar{1}]$ or $[\bar{1}1\bar{1}]$ axis. Consequently, such a stress will induce a polarization in the atomic orientation of carbon interstitialcies. By cooling a sample under stress from $\gtrsim 175$ °C down to room temperature, the two carbon atoms will become essentially locked to their respective ⟨111⟩ axis, but it is important to realize that at room temperature the defect is essentially free to rotate about its respective ⟨111⟩ axis from one Jahn-Teller distortion to another. For $\vec{H} \parallel [110]$, the EPR spectrum at 15 K arising from carbon pairs pinned on the $[\bar{1}\,\bar{1}1]$ axis will consist of two resonances. One resonance will arise from carbon pairs aligned in the (110) plane, and another resonance will arise from carbon pairs aligned in either the (101) or (011) plane. Since these three orientations achieved thermal equilibrium among

TABLE IV. Relationship between the 12 coordinate frames as labeled in the Zeeman spectrum of Fig. 10, the resonances *F*, *G*, *H*, and *I* as labeled in Fig. 6, and the orientation of Si_j ($j=1,2,3,4$) in each coordinate frame. In coordinate frame *k*, the silicon atoms are rearranged by moving silicon atom *j* to site Si_j in Fig. 11. In effect, the whole crystal is rotated along with these atoms.

Orientation of axis invariant under coordinate transformation	Resonance	Coordinate frame	Transformations $j\rightarrow Si_1$	$j\rightarrow Si_2$	$j\rightarrow Si_3$	$j\rightarrow Si_4$
$[\bar{1}\bar{1}1]$	*I*	1	1	2	3	4
	F	6	1	3	4	2
	F	12	1	4	2	3
[111]	*I*	3	2	1	4	3
	F	7	3	1	2	4
	F	11	4	1	3	2
$[1\bar{1}\bar{1}]$	*H*	4	3	4	1	2
	G	5	4	2	1	3
	G	10	2	3	1	4
$[\bar{1}1\bar{1}]$	*H*	2	4	3	2	1
	G	8	2	4	3	1
	G	9	3	2	4	1

themselves, the relative intensities of these two resonances are 1 and 2, respectively. (Carbon pairs pinned on the [111] give the same identical resonances for $\vec{H}\parallel[110]$ because $\vec{H}$ is an axial vector.) Similarly, another distinct pair of resonances exists having relative intensities of 1 and 2 which are associated with carbon pairs on either the $[1\bar{1}\bar{1}]$ or $[\bar{1}1\bar{1}]$ axis. On the basis of this argument, we see that in Fig. 6 resonances *F* and *I*, whose relative intensities are approximately $1:F::1:2$ and are invariant under stress, constitute one distinct pair of resonances, and resonances *G* and *H*, whose relative intensities remain constant under stress, constitute the other distinct pair of resonances. The important point here is that electronic reorientation processes occur between coordinate frames in common with resonances *F* and *I*. The same is true for *G* and *H*. Furthermore, from our analysis in Fig. 10 we know which coordinate frames *F*, *I*, *G*, and *H* are associated with and exactly how each coordinate frame is oriented with respect to the others. This information is tabulated in Table IV. By simply arranging the data in Table IV into subsets consisting of coordinate frames which have been identified by resonances *I*, *F* and *H*, *G* as differing by only an electronic reorientation, one can identify a particular ⟨111⟩ axis which remains fixed under transformations between those three unique coordinate frames. In particular, one sees that for transformations between coordinate frames 1, 6, and 12, which are in common with resonances *I* and *F*, the $[\bar{1}\bar{1}1]$ axis remains fixed. Consequently, the two carbon atoms in coordinate frame 1 are pinned on the $[\bar{1}\bar{1}1]$ axis. By way of contrast, if our stress data had indicated that electronic reorientation processes occurred between coordinate frames in common with resonances *I* and *G*, then the data in Table IV would indicate that the carbon atoms were aligned along the [111] axis in Fig. 11. Thus, the effects due to stress applied at high temperature on the Zeeman spectrum, as evidenced in Fig. 6, indicate according to this analysis that the two carbon atoms lie on the $[\bar{1}\bar{1}1]$ axis as shown in Figs. 11 and 12 and not on the [111] axis.

In Fig. 12, two possible atomic configurations of the carbon interstitialcy are illustrated which correspond to variations in the relative positions of C_α and C_β on the $[\bar{1}\bar{1}1]$ axis. So far we have not been able to discriminate experimentally between these two possibilities. Of course, only one of these two configurations resembles the actual defect.

The Jahn-Teller effect also tells us that the carbon pair is not situated in the middle of a three-vacancy. If sites 3 and 4 in Fig. 11 were vacancies, the defect would necessarily have $\mathfrak{S}_s$ sym-

TABLE V. Classification of the carbon valance orbitals and the silicon ligands in Fig. 11 according to the irreducible representations of the group $\mathfrak{S}_S$.

Irreducible representation	C_k orbitals ($k=\alpha,\beta$)	Silicon ligands
Γ_1	ψ_{2sk}, ψ_{2p_Xk}, ψ_{2p_Zk}	σ_1, σ_2, $\sigma_3+\sigma_4$
Γ_2	ψ_{2p_Yk}	$\sigma_3-\sigma_4$

metry and would not exhibit electronic reorientation effects. This argument can be generalized by saying that the existence of other perturbations in the surrounding lattice (within ≈ 15 Å), e.g., impurities, vacancies, interstitials, which do not preserve the $\mathfrak{C}_{3v}$ symmetry of the Si-*G*11 center without Jahn-Teller effects, is forbidden.

With Jahn-Teller effects, the primitive configuration illustrated in Fig. 11 is distorted to $\mathfrak{C}_s$ symmetry, and it is this distorted configuration which we are forced to look at with EPR. An analysis of the ^{13}C hyperfine interactions in terms of various linear combinations of atomic orbitals consistent with symmetry considerations give us some insight into the nature of the bonding in this defect. In Table V, the various carbon orbitals and silicon ligands are classified according to the various irreducible representations within the group $\mathfrak{C}_s$. In this model, molecular orbitals which transform as Γ_2 would tend to result in π bonding involving ψ_{2p_Y} orbitals between the two carbon atoms. In analogy with separations found in hydrocarbons involving π and σ bonding, one might expect the separation between the carbon atoms in the Si-*G*11 center to be between 1.2 and 1.5 Å.

Linear combinations of carbon orbitals and silicon ligands which transform as Γ_2 result in molecular orbitals with a node in the XZ plane. Since the trace of the ^{13}C hyperfine interactions is not zero for any combination of signs, the paramagnetic electron is not in a state that transforms as Γ_2 but rather in a Γ_1 state. The results of analyzing the ^{13}C hyperfine interactions in terms of $\Psi(\Gamma_1)$ of Eq. (4) are tabulated in Table III. These results indicate that ≈ 25% of the wave function for the paramagnetic electron is localized on C_β and ≲ 2% on C_α. Furthermore, in the vicinity of C_α and C_β, the wave function is ≈ 93 and 99%, respectively, $2p$-like, with the $2p$ orbitals in the XZ plane. The smaller localization of $\Psi(\Gamma_1)$ and the greater admixture of ψ_{2s} on C_α suggest that C_α tends to be neutrally charged and more substitutional-like. On the other hand, the larger localization of $\Psi(\Gamma_1)$ on C_β and the nearly pure p-like character of the wave function on C_β suggest that C_β tends to be positively charged and more interstitial-like.

The remaining ≈ 73% of the wave function is smeared out over neighboring silicon sites. In fact, in silicon samples containing ordinary carbon, we can see four distinct ^{29}Si hyperfine interactions with $|\vec{A}| \lesssim 15 \times 10^{-4}$ cm^{-1}. Although the resolution is not very good, the intensity of these ^{29}Si hyperfine lines suggest that they arise from pairs of equivalent sites.

It is interesting that the ensemble of Si-*G*11 centers appears to consist of isolated defects even though they are formed by neutron irradiation. This observation and the nature of the defect itself suggest that it is formed as a result of a mobile carbon interstitial atom being trapped by a substitutional carbon atom. This pairing effect is also exhibited by Al and Ga; however, the pairing effect for carbon occurs at 100 K,[1] whereas for Al and Ga it occurs at ≈ 500 K.[2] These results suggest that there is a carbon interstitial in silicon which is mobile at ≈ 100 K.

ACKNOWLEDGMENTS

The technical assistance of N. D. Wing with the EPR measurements and his expertise in setting up the digital recording apparatus is very much appreciated. The author also appreciates the contributions which were generously made by M. K. Gleicher, who supplied us with an appropriate copy routine for making our tapes with the CDC 6600, Dr. M. M. Abraham of Oak Ridge National Laboratory, who electron irradiated our samples, and Dr. R. D. Cowan of Los Alamos Scientific Laboratory, who promptly supplied us with Hartree-Fock calculations for C^0 and C^+.

*This work was supported by the U. S. Atomic Energy Commission.

[1]G. D. Watkins, in *Radiation Damage in Semiconductors*, edited by P. Baruch (Dunod, Paris, 1965), p. 97.
[2]G. D. Watkins, IEEE Trans. Nucl. Sci. NS-16, No. 6, 13 (1969).
[3]K. L. Brower, Radiat. Eff. 8, 213 (1971).
[4]D. F. Daly and H. E. Noffke, Radiat. Eff. 10, 191 (1971).
[5]Y. H. Lee, Y. M. Kim, and J. W. Corbett, Radiat. Eff. 15, 77 (1972).
[6]K. L. Brower and W. Beezhold, J. Appl. Phys. 43, 3499 (1972).
[7]S. P. Singhal, Phys. Rev. B 4, 2497 (1971).
[8]S. P. Singhal, Phys. Rev. B 5, 4203 (1972).
[9]G. D. Watkins, R. P. Messmer, C. Weigel, D. Peak, and J. W. Corbett, Phys. Rev. Lett. 27, 1573 (1971).
[10]C. Weigel, D. Peak, J. W. Corbett, G. D. Watkins, R. P. Messmer, Phys. Rev. B 8, 2906 (1973).
[11]K. L. Brower, Phys. Rev. B 1, 1908 (1970).
[12]D. F. Daly and H. E. Noffke, Radiat. Eff. 8, 203 (1971).
[13]L. C. Allen, H. M. Gladney, and S. H. Glarum, J. Chem. Phys. 40, 3135 (1964).
[14]The $\overleftrightarrow{g}$ tensor for the Si-*SL*4 center in terms of the coordinate system in Fig. 9 is $g_{rr} = 2.0165$, $g_{ss} = g_{tt} = 2.0053 \pm 0.0003$, and $\omega = 0 \pm 1°$.
[15]B. Bleaney and K. W. H. Stevens, Rept. Progr. Phys. 18, 108 (1953).
[16]R. D. Cowan (private communication).
[17]G. Wolber, H. Figger, R. A. Haberstroh, and S. Penselin, Z. Phys. 236, 337 (1970).
[18]D. C. Griffin, R. D. Cowan, and K. L. Andrew, Phys. Rev. A 3, 1233 (1971).
[19]R. C. Newman and A. R. Bean, Radiat. Eff. 8, 189 (1971).

[20]G. D. Watkins (private communication).

[21]In principle one ought to be able to identify the particular ⟨111⟩ axis on which the carbon atoms are located by examining the effects of low-temperature stress on the EPR spectrum for $\vec{H} \parallel [111]$. The results of this measurement were inconclusive because the changes in the EPR spectrum were very small and were not proportional to the applied stress. Apparently the difference in the energy of the defect in configurations between which electronic reorientations occur is negligible. We were also unable to observe the Si-G11 spectrum at higher temperatures, where motional effects would be evident in the spectrum because at the higher temperatures we were unable to attain critical coupling to the microwave cavity. Since the defect is observed to be paramagnetic in p-type silicon, the samples do tend to be lossy.

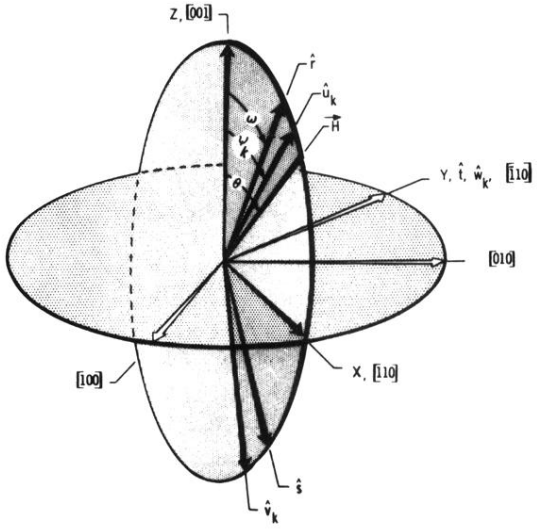

FIG. 9. Definition of the coordinate axes for the $\overleftrightarrow{g}$ and $\overleftrightarrow{A}_k$ tensors in relation to various crystallographic directions.